ECCOMAS Congress 2016
VII European Congress on Computational Methods in Applied Sciences and Engineering
M. Papadrakakis, V. Papadopoulos, G. Stefanou, V. Plevris (eds.)
Crete Island, Greece, 5–10 June 2016

HIGH COMPUTATIONAL EFFICIENCY THROUGH GENERIC ANALYTICAL FORMULATION FOR LINEAR SOIL PRESSURE DISTRIBUTION OF RIGID SPREAD RECTANGULAR FOOTINGS

John Bellos[1] **and Nikolaos P. Bakas**[2]

[1] Assistant Professor
School of Architecture, Engineering, Land & Environmental Sciences, Neapolis University Pafos
j.bellos@nup.ac.cy

[2] Lecturer
School of Architecture, Engineering, Land & Environmental Sciences, Neapolis University Pafos
n.bakas@nup.ac.cy

Keywords: Rectangular footing, soil pressure distribution, analytical solution, vertical loading, biaxial bending, eccentricity regions, compression zone, computational efficiency.

Abstract. *The primary objective of this paper is to resolve and provide generic analytical formulas concerning the linear pressure distribution of rigid spread rectangular footings and, consequently, limit computational costs. All five distinct regions of the eccentricity diagram are related to five possible forms of footing deformations and five discrete shapes of compression zone. For each region, the linear soil pressure distribution in soil-footing interface, the neutral axis position, the maximum pressure and the pressure values at the four corners, are expressed in closed forms as functions of biaxial eccentricities, mean soil pressure and footing dimensions. Several special cases are also presented, verifying the correctness and the consistency of the developed analytical formulas and revealing the physical meaning of the eccentricity diagram. The explicit expressions for responses and resultants enable algorithmic implications without iterations, providing high computational efficiency with low computational cost when forming envelopes for shear forces and bending moment or optimizing the design of footing geometry and footing reinforcement, etc. Through developed computer software, a provided simple example of a rigid spread footing under variable eccentric loading, demonstrates how the theoretical content of this article is used to perform numerical calculations. The software itself comprises 3D visualization technology to facilitate visual examination and validation of the results.*

1 INTRODUCTION

It is well known that rigid spread rectangular footings resting on elastic soils tend to deform in a linearly elastic manner under the action of vertical load and biaxial bending [1, 12]. Such loading conditions may occur either due to eccentric vertical loading or high horizontal excitation as those used for structural design in high seismic risk areas. Thus, assuming footing rigidity of adequately high magnitude, it is reasonable to consider a planar settling of footing base and a linear soil pressure distribution due to constant ratio of pressure to settlement.

The footing-soil interaction generates compression underneath the entire or part of the footing base, depending on the area being in contact with the soil. This area, usually called *active area* or *effective area* or *compression zone* [3, 11, 13], should not be less than a certain percentage of the entire base area. In fact, when the effective eccentricities, computed by dividing bending moments with vertical force, lay outside a certain geometric ellipse called *secondary core*, the active area is smaller than half the base area. As strictly as required by regulations and usually recommended by good practice, such cases are not acceptable in footing design.

The most important issue concerning rectangular footings is optimal geometric and reinforcement design [2, 3, 6, 7, 14]. Initially, a set of suitable values is chosen so that, under serviceability conditions, the maximum pressure exerted at any footing position does not exceed the soil bearing capacity. Moreover, constraints set for enveloped bending, shearing and punching should not be violated under ultimate loading conditions, while requirements imposed by regulations should be fully met. All the above involve an immense amount of intensive calculations through complex iterative processes. Several procedures were developed in the past for handling efficiently such footing-soil interaction problems, by using either analytical [2, 4, 5, 6, 7, 13, 14], numerical [10, 11], graphical [3, 15], or hybrid techniques [8, 9]. Although accurate and useful, some of them are rather computationally expensive, while others are not so wide-ranging or not easily implementable in designing footings of such specific shape, yet participating in a complex structure assembly subject to various loading actions. On the other hand, the generic explicit formulas presented in this article increase the efficiency of the required design processes by reducing considerably the computational costs.

Another advantage of the presented analytical method is that, instead of relating eccentricities to external loading conditions, they are evaluated by using reaction resultants at the respective support node as derived from the space frame model of the structure. Hence, these effective eccentricities express a clear relation of biaxial bending moments to vertical load for the specific footing, since they are not directly associated with external loading and influences from neighboring columns, footings and connecting beams.

This paper attempts to enlighten the issues concerning the rigid spread rectangular footings by providing easily programmable analytical formulas and, through a developed intelligent software and 3D visualization technology, facilitate results inspection, confirm engineering intuition, unshed light to foundation settlement and encourage future research in related fields.

2 THE MATHEMATICAL MODEL

As we stated previously, a rigid spread rectangular footing is expected to deform in a planar manner. Therefore, it is reasonable to consider a linear soil pressure distribution underneath the base, that is

$$p(x, y) = p_{\max} \cdot \left(-\frac{x}{x_n} - \frac{y}{y_n} + 1 \right) \tag{1}$$

where p_{max} is the maximum soil pressure on the base and x_n, y_n are the intercepts of the neutral axis determining the active area of the footing (see Figure 1).

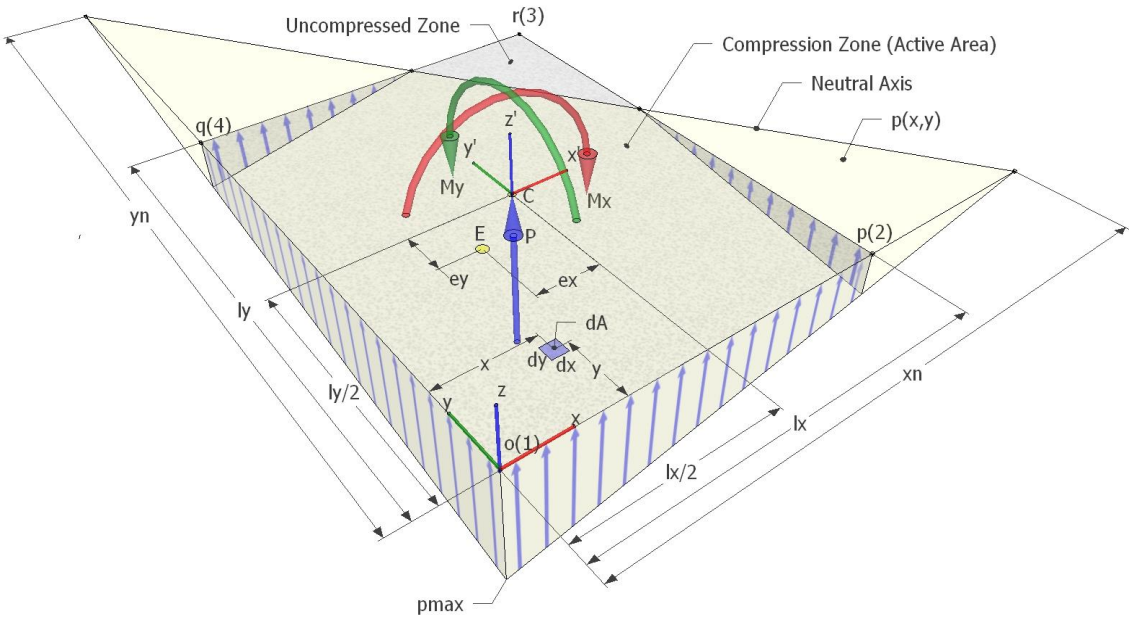

Figure 1: Linear soil pressure distribution on a rigid spread rectangular footing.

The effective eccentricities from the footing center, derived from certain reaction resultants at the central support node, i.e. the calculated values of biaxial moments M_x, M_y and vertical force P (see Figure 1), are expressed as

$$e_x = \frac{M_x}{P}, \qquad e_y = \frac{M_y}{P} \tag{2}$$

Equilibrium of actions and reactions at the base center (x_c, y_c) requires

$$P = \iint_A p(x,y) \cdot dA \tag{3}$$

$$M_x = \iint_A (x_c - x) \cdot p(x,y) \cdot dA \tag{4}$$

$$M_y = \iint_A (y_c - y) \cdot p(x,y) \cdot dA \tag{5}$$

Substituting equation (3) into equations (4) and (5), they are transformed into

$$M_x = P \cdot x_c - \iint_A x \cdot p(x,y) \cdot dA \Rightarrow P \cdot (x_c - e_x) = \iint_A x \cdot p(x,y) \cdot dA \tag{6}$$

$$M_y = P \cdot y_c - \iint_A y \cdot p(x,y) \cdot dA \Rightarrow P \cdot (y_c - e_y) = \iint_A y \cdot p(x,y) \cdot dA \tag{7}$$

The mean soil pressure on a footing with dimensions l_x, l_y is defined as

$$p_m = \frac{P}{l_x \cdot l_y} \tag{8}$$

If, by convention, one uses absolute values for eccentricities and thus presets the maximum soil pressure at the lower left footing corner, i.e. $p_o = p_{max}$ (see Figure 1). Then equations (3), (6) and (7) can be written as

$$p_m \cdot l_x \cdot l_y = \iint_A p(x, y) \cdot dx \cdot dy \tag{9}$$

$$p_m \cdot l_x \cdot l_y \cdot \left(\frac{l_x}{2} - |e_x| \right) = \iint_A x \cdot p(x, y) \cdot dx \cdot dy \Rightarrow p_m \cdot l_x^2 \cdot l_y \cdot \left(\frac{1}{2} - \frac{|e_x|}{l_x} \right) = \iint_A x \cdot p(x, y) \cdot dx \cdot dy \tag{10}$$

$$p_m \cdot l_x \cdot l_y \cdot \left(\frac{l_y}{2} - |e_y| \right) = \iint_A y \cdot p(x, y) \cdot dx \cdot dy \Rightarrow p_m \cdot l_x \cdot l_y^2 \cdot \left(\frac{1}{2} - \frac{|e_y|}{l_y} \right) = \iint_A y \cdot p(x, y) \cdot dx \cdot dy \tag{11}$$

There is a direct relation of pressure values at actual footing corners with those computed from at rearranged footing corners, with the order strictly depending on the eccentricities signs, i.e.

$$\begin{aligned}
&e_x \geq 0 \,\&\, e_y \geq 0 \Rightarrow p_1 = p_o = p_{\max},\ p_2 = p_p,\ p_3 = p_r,\ p_4 = p_q \\
&e_x < 0 \,\&\, e_y > 0 \Rightarrow p_1 = p_p,\ p_2 = p_o = p_{\max},\ p_3 = p_q,\ p_4 = p_r \\
&e_x \leq 0 \,\&\, e_y < 0 \Rightarrow p_1 = p_r,\ p_2 = p_q,\ p_3 = p_o = p_{\max},\ p_4 = p_p \\
&e_x > 0 \,\&\, e_y < 0 \Rightarrow p_1 = p_q,\ p_2 = p_r,\ p_3 = p_p,\ p_4 = p_o = p_{\max}
\end{aligned} \tag{12}$$

Solving the system of equations (9), (10) and (11) and determining the unknown parameters x_n, y_n and p_{max}, then the equation (1) depends on the signs of effective eccentricities and, therefore, it can be rewritten as

$$p(x, y) = p_{\max} \cdot \left[- sign(e_x) \cdot \frac{x}{x_n} - sign(e_y) \cdot \frac{y}{y_n} + 1 \right] \tag{13}$$

and by relocating the origin of the coordinate system at the footing centroid, the linear soil pressure distribution can be written in an equivalent to equation (1) expression, that is

$$p(x', y') = p_{\max} \cdot \left[- sign(e_x) \cdot \frac{x'}{x_n} - sign(e_y) \cdot \frac{y'}{y_n} + 1 - \frac{1}{2} \left(\frac{l_x}{x_n} + \frac{l_y}{y_n} \right) \right] \tag{14}$$

3 THE ECCENTRICITY DIAGRAM

As effective eccentricities, evaluated using equations (2), sweep the rectangular footing base certain types of deformation occur, thus generating an *eccentricity diagram* for each footing, as presented in Figure 2. This diagram, also obtained by other authors using different approaches [13], constitutes a very strong practical tool for determining the form of pressure distribution expected under certain loading conditions. In this work, the border lines on the eccentricity diagram are provided explicitly while special cases reveal their physical meaning.

There are five distinct regions in this diagram, namely A-E, corresponding to different types of deformation and active areas of unique geometric shapes (see Figure 2). Each regional case is subdivided into four subcases, each associated with one primary footing corner of maximum soil pressure, as determined by eccentricities signs in equations (12). Notice that there is a rhombus domain, usually called *main core*, having semi-diagonals equal to 1/6 of the respective footing lengths and a surrounding elliptic domain, usually called *secondary*

core, bounded by an ellipse with major and minor semi-axes equal to 1/3 of the respective footing lengths (dashed line in Figure 2). The first contains the entire regions C, while the second comprises regions B and certain parts of regions D and E. The remaining parts of regions D and E and the entire regions A are excluded, since corresponded to active areas smaller than half the footing base area. Regulations as well as good practice require that effective eccentricities should remain inside the secondary core in order to maintain an acceptable footing design.

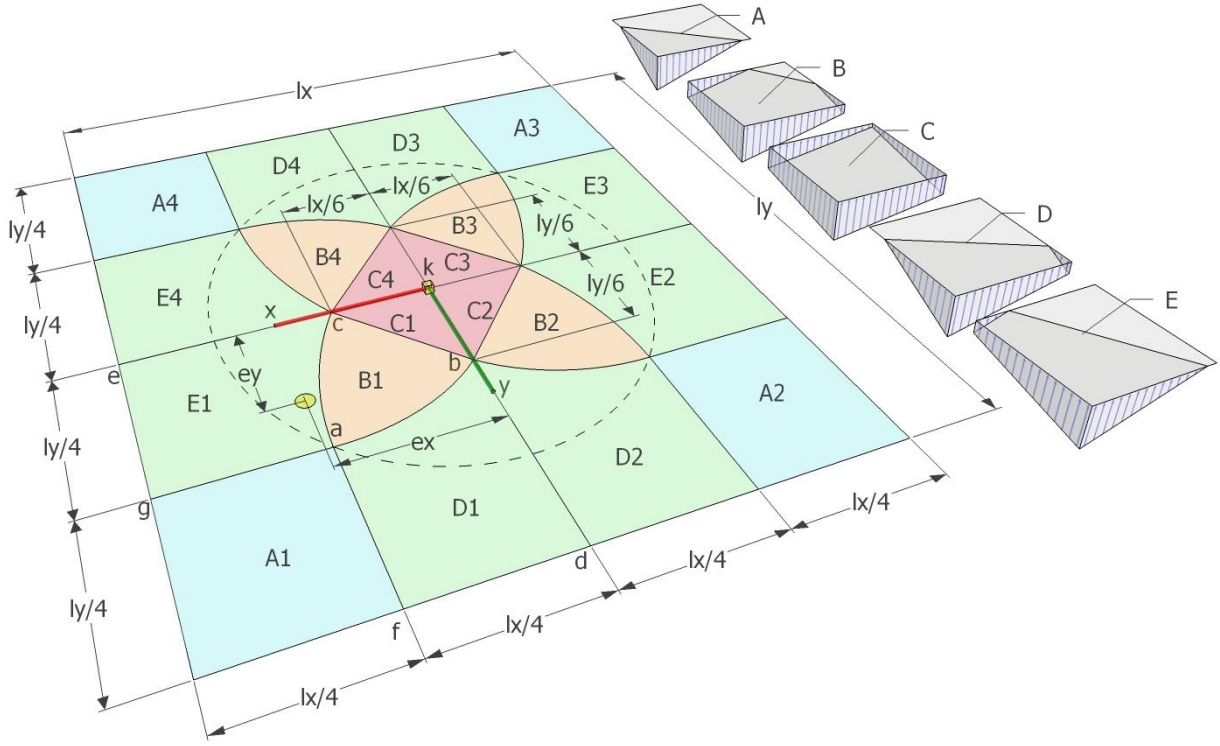

Figure 2: The eccentricity diagram of a rigid spread rectangular footing.

4 THE ECCENTRICITY REGIONS

The analytical formulas for all five regions are presented in the subsections below. They are produced by integrating the equations (9), (10) and (11) over the active area of the footing base corresponding to each regional case. Nevertheless, for saving space and time, the detailed development process of the formulas is not provided here.

4.1 Region C: Full Compression Zone

Regions C corresponds to four equal right triangles composing a rhombus shape with semi-diagonals equal to 1/6 of the respective footing lengths (see Figure 3). This rhombus area, usually called main core, represents small eccentricities generated by vertical forces applied at points in it and capable of setting the entire footing base under compression. Maximum pressure occurs at the footing corner corresponding to the right triangle enclosing the eccentricity point.

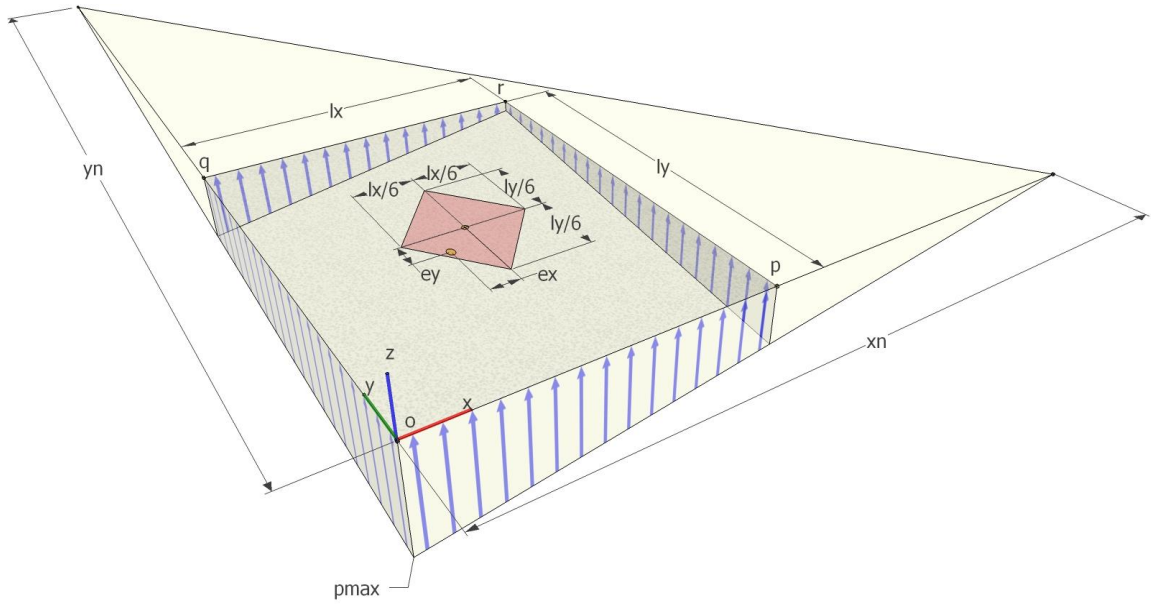

Figure 3: Full compression zone.

The intercepts of the neutral axis are given by

$$x_n = l_x \cdot \left(1+6\cdot\frac{|e_x|}{l_x}+6\cdot\frac{|e_y|}{l_y}\right)\Bigg/\left(12\cdot\frac{|e_x|}{l_x}\right), \qquad y_n = l_y \cdot \left(1+6\cdot\frac{|e_x|}{l_x}+6\cdot\frac{|e_y|}{l_y}\right)\Bigg/\left(12\cdot\frac{|e_y|}{l_y}\right) \quad (15)$$

The maximum soil pressure at the primary corner of the footing base (coordinate system origin O) along with the soil pressure at the rest corners, are provided by the equations

$$\begin{aligned} p_o &= p_{\max} = p_m \cdot \left(1+6\cdot\frac{|e_x|}{l_x}+6\cdot\frac{|e_y|}{l_y}\right), & p_p &= p_m \cdot \left(1-6\cdot\frac{|e_x|}{l_x}+6\cdot\frac{|e_y|}{l_y}\right), \\ p_q &= p_m \cdot \left(1+6\cdot\frac{|e_x|}{l_x}-6\cdot\frac{|e_y|}{l_y}\right), & p_r &= p_{\min} = p_m \cdot \left(1-6\cdot\frac{|e_x|}{l_x}-6\cdot\frac{|e_y|}{l_y}\right) \end{aligned} \quad (16)$$

In this particular case, since the active area is the entire footing base, all footing corners should be under compression, i.e. $p_o \geq 0$ & $p_p \geq 0$ & $p_q \geq 0$ & $p_r \geq 0$. Since p_r represents the minimum compression value, the last of equations (16) yields the rhombus shape boundary for regions C shown in Figure 3, i.e.

$$\frac{|e_x|}{l_x}+\frac{|e_y|}{l_y} \leq \frac{1}{6} \quad (17)$$

4.2 Region A: Triangular Compression Zone

Regions A corresponds to four smaller corner rectangles, each having sides equal to 1/4 of the respective footing lengths (see Figure 4). They represent excessive eccentricities generated by vertical forces applied at points inside these corner rectangles, imposing high pressure to respective triangular compression zones of the footing base. Maximum pressure occurs at the footing corner associated with the corner rectangle enclosing the eccentricity point.

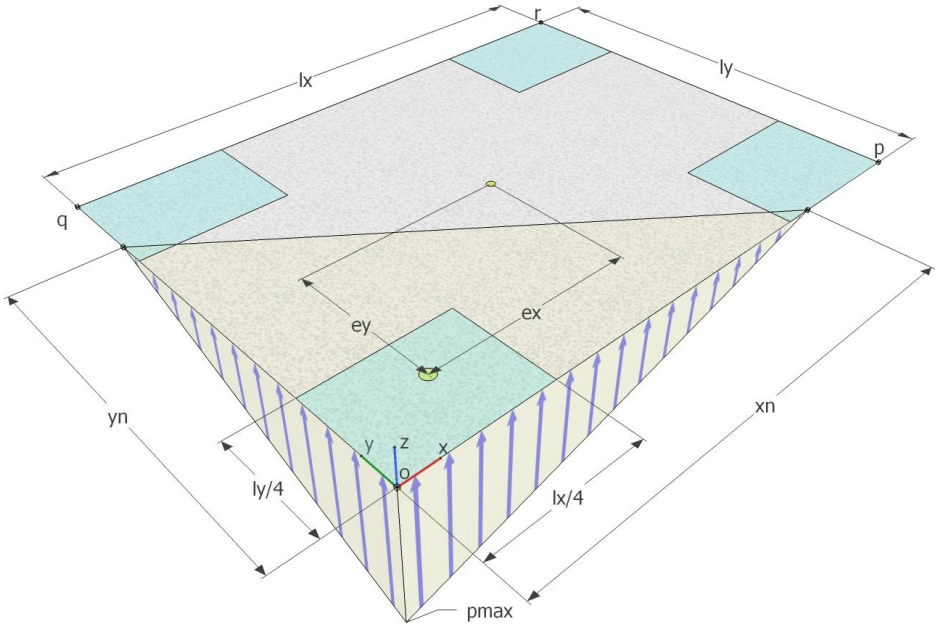

Figure 4: Triangular compression zone.

The neutral axis intercepts are given by

$$x_n = 4 \cdot l_x \cdot \left(\frac{1}{2} - \frac{|e_x|}{l_x} \right), \qquad y_n = 4 \cdot l_y \cdot \left(\frac{1}{2} - \frac{|e_y|}{l_y} \right) \tag{18}$$

The soil pressure values at the footing corners are provided by

$$p_o = p_{\max} = \frac{3 \cdot p_m}{8 \cdot \left(\frac{1}{2} - \frac{|e_x|}{l_x} \right) \cdot \left(\frac{1}{2} - \frac{|e_y|}{l_y} \right)}, \qquad p_p = p_q = p_r = p_{\min} = 0 \tag{19}$$

For triangular compression zone the intercepts should be confined within the neighboring sides of the footing base. Hence, equations (18) yield the rectangular shape boundary for region A (see Figure 4), expressed as the lower and upper bounds in the two inequalities

$$\begin{aligned} 0 < x_n \le l_x \Rightarrow \qquad & \frac{1}{4} \le \frac{|e_x|}{l_x} < \frac{1}{2} \\ 0 < y_n \le l_y \Rightarrow \qquad & \frac{1}{4} \le \frac{|e_y|}{l_y} < \frac{1}{2} \end{aligned} \tag{20}$$

where the upper bounds denote that eccentricities outside the footing base are unbalanced.

4.3 Region D: Trapezoidal Compression Zone in x-Direction

Regions D corresponds to four curved trapezoids attached to the x-direction footing sides in pairs, each having bases equal to 1/3 and 1/4 of the y-direction footing length respectively, altitude 1/4 of the x-direction footing length and a curved side (see Figure 5). They represent large eccentricities generated by vertical forces applied at points inside these curved trapezoids, imposing pressure to respective trapezoidal zones covering the entire x-direction foot-

ing side. Maximum pressure occurs at the footing corner corresponding to the curved trapezoid enclosing the eccentricity point.

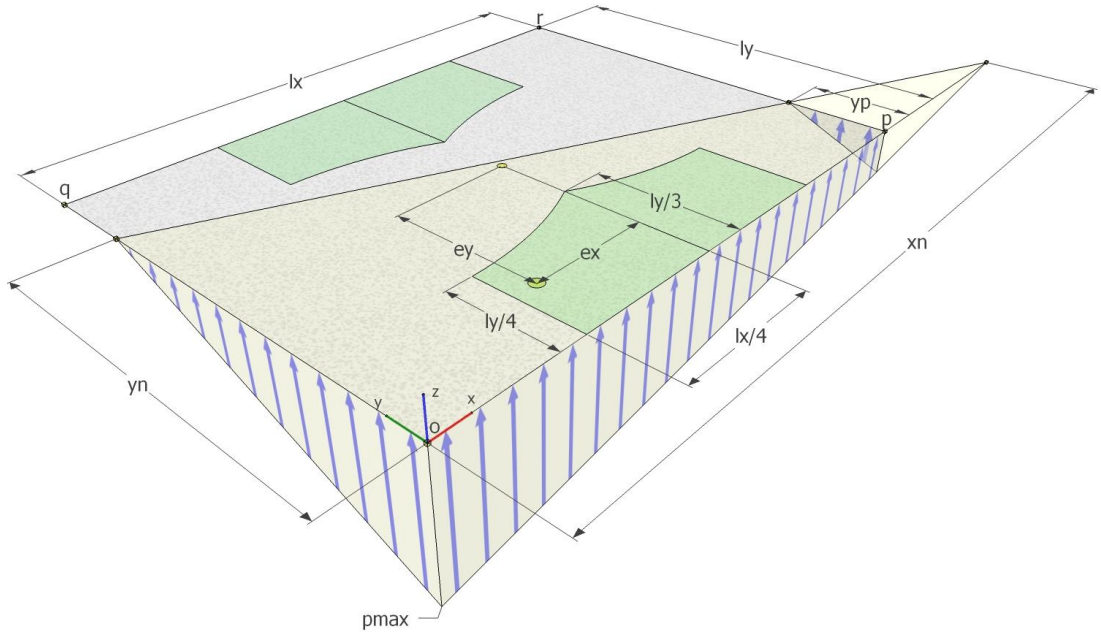

Figure 5: Trapezoidal compression zone covering the entire side in x-direction.

The neutral axis position, determined by its intercepts and its trace y_p on the parallel side (see Figure 5), is provided by

$$x_n = l_x \cdot \left(1+6\cdot\frac{|e_x|}{l_x}+\sqrt{1-12\cdot\frac{e_x^2}{l_x^2}}\right)\Bigg/\left(12\cdot\frac{|e_x|}{l_x}\right),$$
$$y_n = \frac{1}{2}\cdot l_y \cdot \left(\frac{1}{2}-\frac{|e_y|}{l_y}\right)\cdot\left(2+\sqrt{1-12\cdot\frac{e_x^2}{l_x^2}}\right)\cdot\left(1+2\cdot\frac{|e_x|}{l_x}-\sqrt{1-12\cdot\frac{e_x^2}{l_x^2}}\right)\Bigg/\left[\frac{|e_x|}{l_x}\cdot\left(1+4\cdot\frac{e_x^2}{l_x^2}\right)\right], \quad (21)$$
$$y_p = y_n\cdot\left(1-\frac{l_x}{x_n}\right)$$

The soil pressure values at the footing corners are

$$p_o = p_{\max} = \frac{p_m}{3}\cdot\left(2-\sqrt{1-12\cdot\frac{e_x^2}{l_x^2}}\right)\cdot\left(1+6\cdot\frac{|e_x|}{l_x}+\sqrt{1-12\cdot\frac{e_x^2}{l_x^2}}\right)\Bigg/\left(\frac{1}{2}-\frac{|e_y|}{l_y}\right),$$
$$p_p = p_{\max}\cdot\left(1-\frac{l_x}{x_n}\right), \qquad p_q = p_r = p_{\min} = 0 \quad (22)$$

Requiring the x-intercept to lie on the extension of the respective footing side, the bases of the trapezoidal region are given as the lower and upper bounds of an inequality, i.e.

$$1 \le \frac{x_n}{l_x} \Rightarrow \qquad 0 \le \frac{|e_x|}{l_x} \le \frac{1}{4} \quad (23)$$

In fact, the upper bound of the inequality guaranties that the discriminant, appearing under the square roots of equations (21) and (22), is always positive definite.

Confining the y-intercept within the respective footing side, the lateral sides of the trapezoidal region are given as the lower and upper bounds of another inequality (see Figure 5)

$$0<\frac{y_n}{l_y}\le 1\Rightarrow \qquad \frac{1}{2}-\frac{1}{6}\cdot\left(2-\sqrt{1-12\cdot\frac{e_x^2}{l_x^2}}\right)\cdot\left(1+2\cdot\frac{|e_x|}{l_x}+\sqrt{1-12\cdot\frac{e_x^2}{l_x^2}}\right)\Bigg/\left(1+4\cdot\frac{|e_x|}{l_x}\right)\le\frac{|e_y|}{l_y}<\frac{1}{2} \quad (24)$$

Here, the lower bound of the inequality expresses the curved side of trapezoid while the upper bound states that eccentricities outside the footing base are unbalanced.

4.4 Region E: Trapezoidal Compression Zone in y-Direction

Regions E corresponds to four curved trapezoids attached to the y-direction footing sides in pairs, each having bases equal to 1/3 and 1/4 of the y-direction footing length respectively, altitude 1/4 of the y-direction footing length and a curved side (see Figure 6). They represent large eccentricities generated by vertical forces applied at points inside these curved trapezoids, imposing pressure to respective trapezoidal compression zones covering the entire y-direction footing side. Maximum pressure occurs at the footing corner corresponding to the curved trapezoid enclosing the eccentricity point.

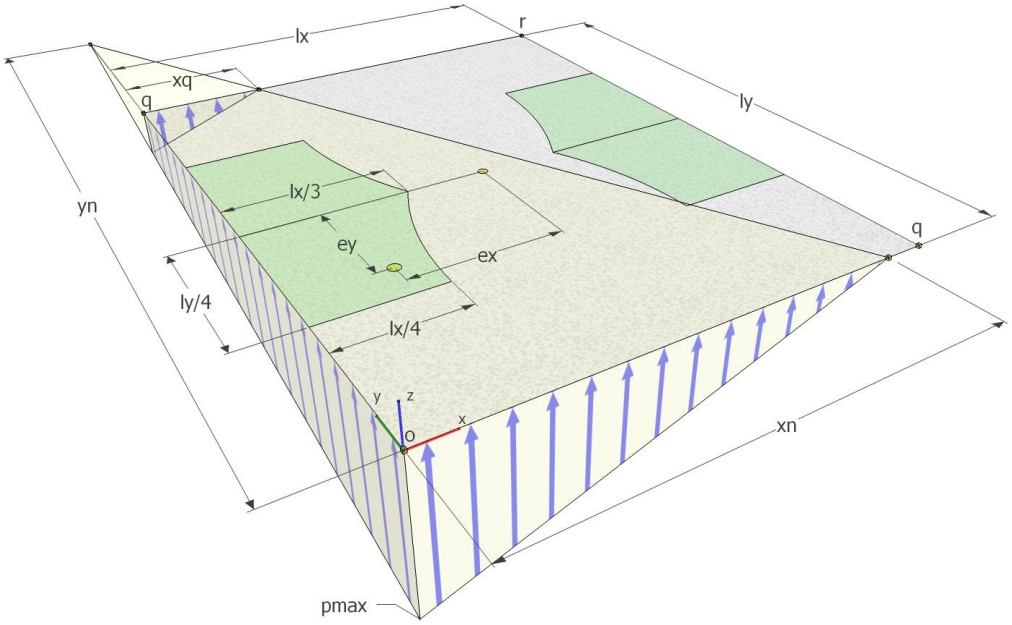

Figure 6: Trapezoidal compression zone covering entire side in y-direction.

The position of the neutral axis is provided by

$$x_n=\frac{1}{2}\cdot l_x\cdot\left(\frac{1}{2}-\frac{|e_x|}{l_y}\right)\cdot\left(2+\sqrt{1-12\cdot\frac{e_y^2}{l_y^2}}\right)\cdot\left(1+2\cdot\frac{|e_y|}{l_y}-\sqrt{1-12\cdot\frac{e_y^2}{l_y^2}}\right)\Bigg/\left[\frac{|e_y|}{l_y}\cdot\left(1+4\cdot\frac{e_y^2}{l_y^2}\right)\right],$$

$$y_n=l_y\cdot\left(1+6\cdot\frac{|e_y|}{l_y}+\sqrt{1-12\cdot\frac{e_y^2}{l_y^2}}\right)\Bigg/\left(12\cdot\frac{|e_y|}{l_y}\right),\qquad x_q=x_n\cdot\left(1-\frac{l_y}{y_n}\right) \quad (25)$$

The soil pressure values at the footing corners are

$$p_o = p_{\max} = \frac{p_m}{3}\cdot\left(2-\sqrt{1-12\cdot\frac{e_y^2}{l_y^2}}\right)\cdot\left(1+6\cdot\frac{|e_y|}{l_y}+\sqrt{1-12\cdot\frac{e_y^2}{l_y^2}}\right)\Bigg/\left(\frac{1}{2}-\frac{|e_x|}{l_x}\right),$$
$$p_q = p_{\max}\cdot\left(1-\frac{l_y}{y_n}\right), \qquad p_p = p_r = p_{\min} = 0 \tag{26}$$

Confining properly the intercepts of neutral axis with respect to footing sides in equations (25), the curved trapezoid is determined by the following two inequalities

$$0<\frac{x_n}{l_x}\le 1 \Rightarrow \qquad \frac{1}{2}-\frac{1}{6}\cdot\left(2-\sqrt{1-12\cdot\frac{e_y^2}{l_y^2}}\right)\cdot\left(1+2\cdot\frac{|e_y|}{l_y}+\sqrt{1-12\cdot\frac{e_y^2}{l_y^2}}\right)\Bigg/\left(1+4\cdot\frac{|e_y|}{l_y}\right)\le\frac{|e_x|}{l_x}<\frac{1}{2}$$
$$1\le\frac{y_n}{l_y}\Rightarrow \qquad 0\le\frac{|e_y|}{l_y}\le\frac{1}{4} \tag{27}$$

The bounds of the first inequality express the lateral sides of the curved trapezoid while the bounds of the second its bases.

4.5 Region B: Pentagonal Compression Zone

Regions B corresponds to four diagonally placed curved triangles, each having two curved sides and one flat base, as shown in Figure 7. These curved triangles form part of the secondary core, inscribed in its elliptic boundary and surrounding the main core (see Figure 2). They represent moderate eccentricities generated by vertical forces applied at points inside them, imposing pressure to respective pentagonal compression zones while preserving a triangular uncompressed zone. Maximum pressure occurs at the footing corner corresponding to the curved triangle enclosing the eccentricity point.

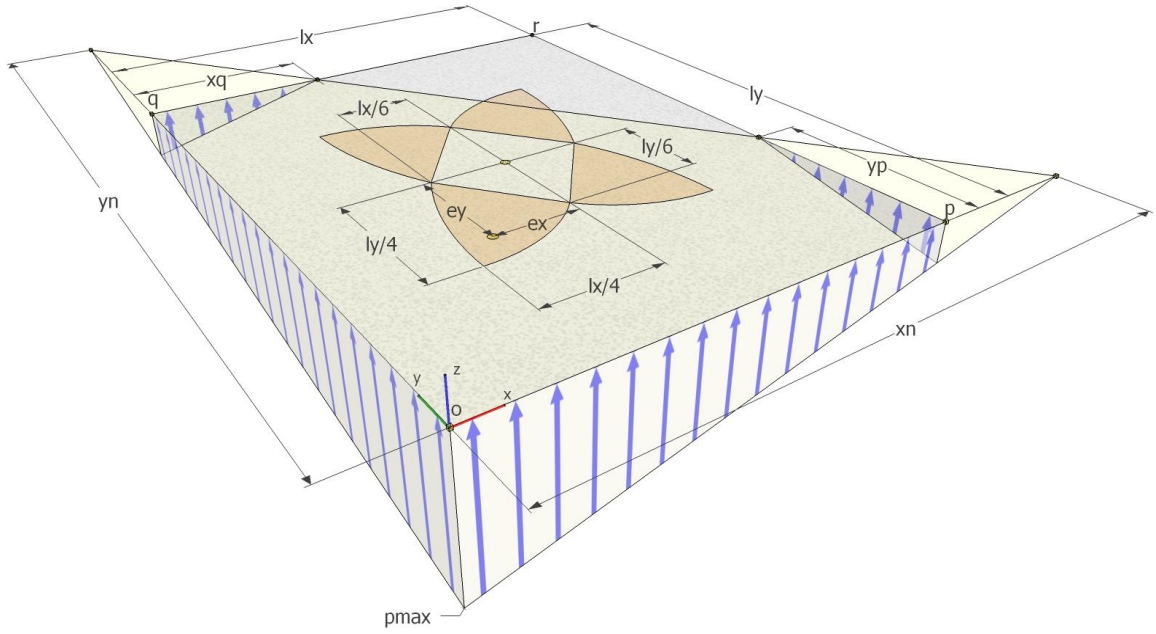

Figure 7: Pentagonal compression zone (triangular uncompressed zone).

As shown below, in full agreement with other sources [13], in this case the solution cannot be expressed in closed form. In fact, the intercepts of the neutral axis are provided by recursive formulas, i.e.

$$x_n = 4\cdot l_x\cdot\left(\frac{1}{2}-\frac{|e_x|}{l_x}\right)\cdot\frac{1-\left(1-\frac{l_x}{x_n}\right)^3-\left(1-\frac{l_y}{y_n}\right)^3}{1-\left(1-\frac{l_x}{x_n}\right)^4-\left(1-\frac{l_y}{y_n}\right)^4-4\cdot\left(1-\frac{l_x}{x_n}\right)^3\cdot\frac{l_x}{x_n}},$$
$$y_n = 4\cdot l_y\cdot\left(\frac{1}{2}-\frac{|e_y|}{l_y}\right)\cdot\frac{1-\left(1-\frac{l_x}{x_n}\right)^3-\left(1-\frac{l_y}{y_n}\right)^3}{1-\left(1-\frac{l_x}{x_n}\right)^4-\left(1-\frac{l_y}{y_n}\right)^4-4\cdot\left(1-\frac{l_y}{y_n}\right)^3\cdot\frac{l_y}{y_n}} \tag{28}$$

One can easily prove, either numerically or algebraically, that the set of equations (27) constitutes a fast converging iterative procedure. Consequently, once the intercept values found they are substituted to all consequent equations.

The traces of the neutral axis on the two opposite footing sides, as shown in Figure 7, are

$$y_p = y_n\cdot\left(1-\frac{l_x}{x_n}\right),\qquad x_q = x_n\cdot\left(1-\frac{l_y}{y_n}\right) \tag{29}$$

The soil pressure values at the footing corners are

$$p_o = p_{\max} = \frac{6\cdot p_m\cdot\frac{l_x}{x_n}\cdot\frac{l_y}{y_n}}{1-\left(1-\frac{l_x}{x_n}\right)^3-\left(1-\frac{l_y}{y_n}\right)^3},$$
$$p_p = p_{\max}\cdot\left(1-\frac{l_x}{x_n}\right),\qquad p_q = p_{\max}\cdot\left(1-\frac{l_y}{y_n}\right),\qquad p_r = p_{\min} = 0 \tag{30}$$

Since, on its limits, region B degenerates to regions C, D and E respectively, the boundary of the curved triangle is clearly determined by the set of three inequalities

$$\frac{|e_x|}{l_x}+\frac{|e_y|}{l_y}\ge\frac{1}{6}$$
$$\frac{|e_x|}{l_x}\le\frac{1}{2}-\frac{1}{6}\cdot\left(2-\sqrt{1-12\cdot\frac{e_y^2}{l_y^2}}\right)\cdot\left(1+2\cdot\frac{|e_y|}{l_y}+\sqrt{1-12\cdot\frac{e_y^2}{l_y^2}}\right)\Bigg/\left(1+4\cdot\frac{|e_y|}{l_y}\right) \tag{31}$$
$$\frac{|e_y|}{l_y}\le\frac{1}{2}-\frac{1}{6}\cdot\left(2-\sqrt{1-12\cdot\frac{e_x^2}{l_x^2}}\right)\cdot\left(1+2\cdot\frac{|e_x|}{l_x}+\sqrt{1-12\cdot\frac{e_x^2}{l_x^2}}\right)\Bigg/\left(1+4\cdot\frac{|e_x|}{l_x}\right)$$

The first inequality represents eccentricities outside the main core of rhombus region C, while the rest represent eccentricities inside the secondary zone bound by the curved sides of the trapezoidal regions D and E respectively (see Figure 2), as derived in the respective chapters.

5 SPECIAL CASES

Several borderline cases are represented here, verifying the correctness and the consistency of the developed analytical formulas, reassuring the regional continuity and revealing the physical meaning of the eccentricity diagram.

5.1 One-way Eccentricity in Region C

Imposing x-direction eccentricity in Region C by setting $e_y = 0$, as shown in Figure 8, equations (15) and (16) yield the well-known formulas for soil pressure distribution of single slope

$$x_n = l_x \cdot \left(1+6\cdot\frac{|e_x|}{l_x}\right) \Big/ \left(12\cdot\frac{|e_x|}{l_x}\right), \qquad y_n = \infty \tag{32}$$

$$p_o = p_q = p_{\max} = p_m \cdot \left(1+6\cdot\frac{|e_x|}{l_x}\right), \qquad p_p = p_r = p_{\min} = p_m \cdot \left(1-6\cdot\frac{|e_x|}{l_x}\right) \tag{33}$$

while inequality (17) diminishes to representing segment ‘kc’, that is

$$\frac{|e_x|}{l_x} < \frac{1}{6} \tag{34}$$

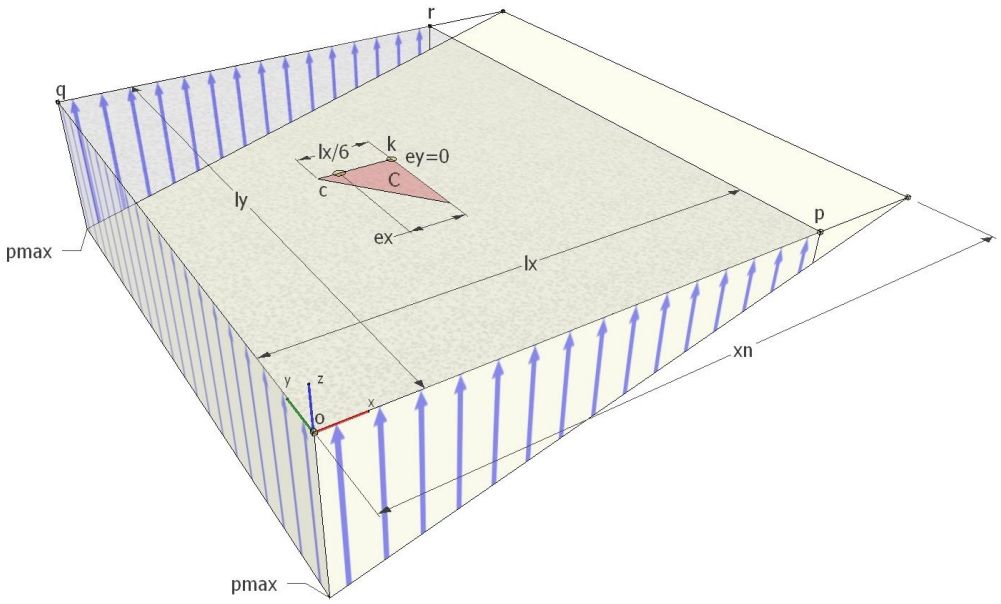

Figure 8: Soil pressure distribution for one-way eccentricity in segment 'kc'.

5.2 One-way Eccentricity in Region C

Imposing x-direction eccentricity in Region E by setting $e_y = 0$, as shown in Figure 9, equations (25) and (26) yield the well-known formulas for soil pressure distribution of single slope and limited active area

$$x_n = 3\cdot l_x \cdot \left(\frac{1}{2}-\frac{|e_x|}{l_x}\right), \qquad y_n = \infty \tag{35}$$

$$p_o = p_q = p_{\max} = \frac{2}{3} \cdot p_m \Big/ \left(\frac{1}{2} - \frac{|e_x|}{l_x} \right), \qquad p_p = p_r = p_{\min} = 0 \tag{36}$$

while inequality (27) diminishes to representing segment ‘ce’, that is

$$\frac{1}{6} \le \frac{|e_x|}{l_x} < \frac{1}{2} \tag{37}$$

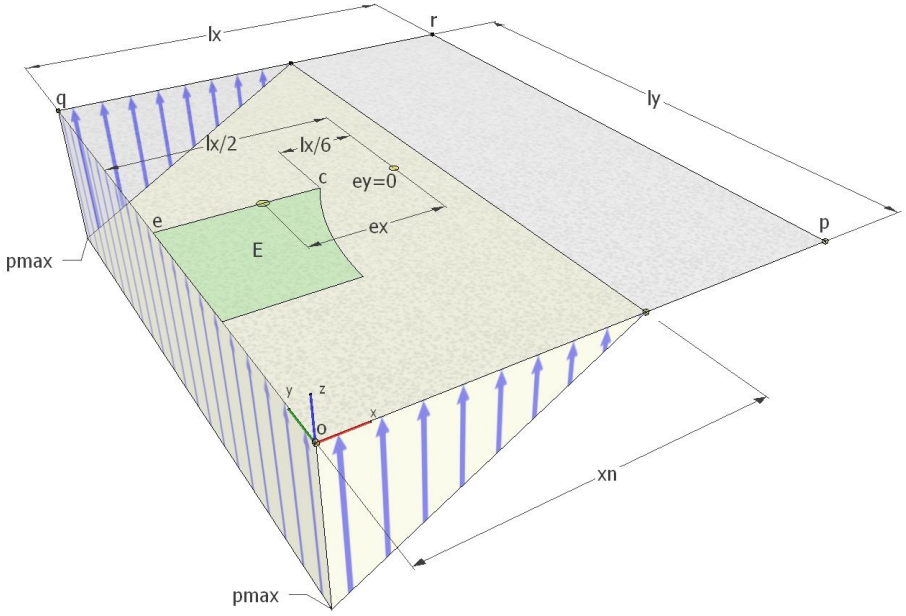

Figure 9: Soil pressure distribution for one-way eccentricity in segment 'ce'.

5.3 One-way Eccentricity in Junction of Regions C, E and B

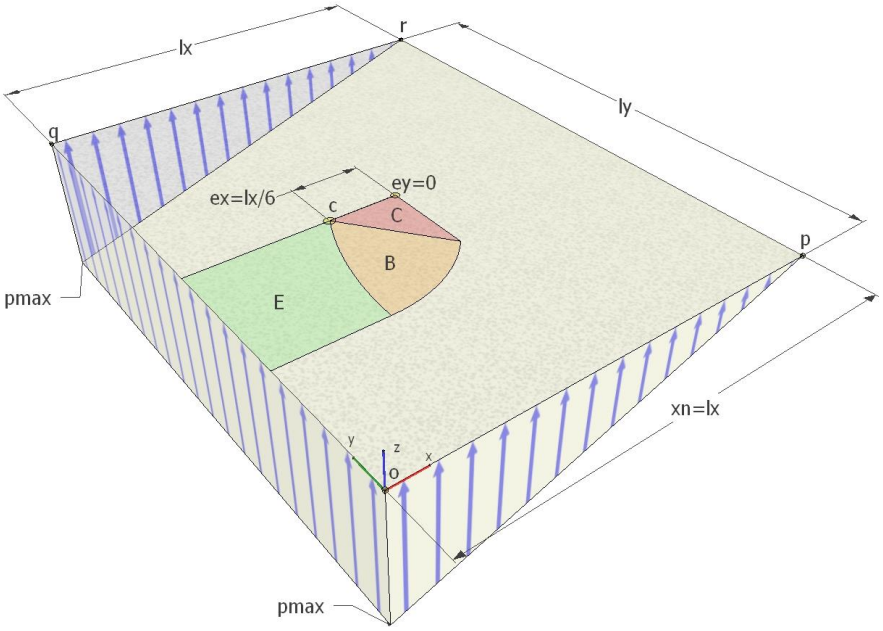

Figure 10: Soil pressure distribution for one-way eccentricity in point 'c'.

Applying x-direction eccentricity in point ‘c’, as shown in Figure 10, by setting

$$\frac{|e_x|}{l_x} = \frac{1}{6}, \qquad e_y = 0 \tag{38}$$

the equations (15) and (16) of region C, (25) and (26) of region E, and (28) and (30) of region B, yield identical results

$$x_n = l_x, \qquad y_n = \infty \tag{39}$$

$$p_o = p_q = p_{\max} = 2 \cdot p_m, \qquad p_p = p_r = p_{\min} = 0 \tag{40}$$

In such a case, the soil pressure distribution of single slope has its neutral axis coincide with the footing base side in y-direction, as illustrated in Figure 10.

5.4 Biaxial Eccentricity in Junction of Regions A, D, E and B

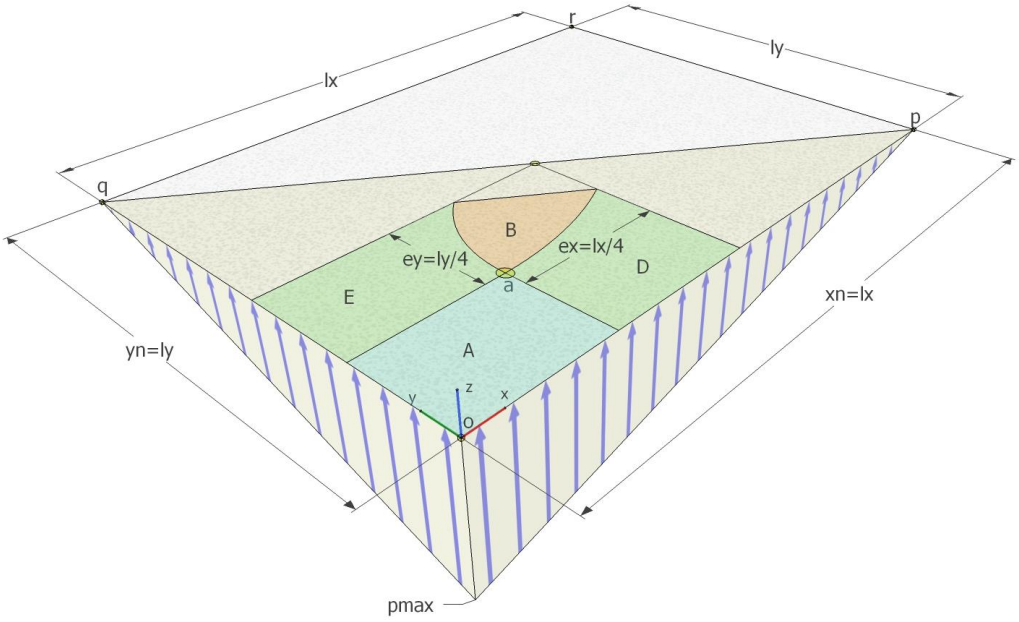

Figure 11: Soil pressure distribution for eccentricity in point 'a'.

Applying biaxial eccentricity in point ‘a’, as shown in Figure 11, by setting

$$\frac{|e_x|}{l_x} = \frac{1}{4}, \qquad \frac{|e_y|}{l_y} = \frac{1}{4} \tag{41}$$

the equations (18) and (19) of region A, (21) and (22) of region D, (25) and (26) of region E, and (28) and (30) of region B, yield identical results

$$x_n = l_x, \qquad y_n = l_y \tag{42}$$

$$p_o = p_{\max} = 6 \cdot p_m, \qquad p_p = p_q = p_r = p_{\min} = 0 \tag{43}$$

In such a case, the soil pressure distribution has its neutral axis coincide with the respective diagonal of the orthogonal base, as illustrated in Figure 11.

6 APPLICATION AND DISCUSSION

A simple example is provided here to demonstrate how the generic analytical formulas of this article are used to perform numerical calculations via developed computer software, thus offering high computational efficiency by limiting computational costs. The software itself comprises a 3D visualization module, facilitating visual examination and validation of the results. Note that all figures and tables of this example have been produced through this software and can be reproduced by rerunning it, practically offering an infinite number of variations to the researcher/engineer.

The structural model concerns a 0.25mx0.25m square column of height 3.00m fixed to a 1.00mx1.00m rigid spread square footing of depth 0.50m. The material used is concrete C30/37 reinforced with steel B500C, with safety factors 1.50 and 1.15 for concrete and steel respectively, and applied with covering of 0.03m for the column and 0.065 for the footing.

The central footing studied for variable eccentric loading required by building codes. Eurocode 1 (EN1991, EC1), Eurocode 2 (EN1992, EC2) and Eurocode 8 (EN1998, EC8) applied in our case, complemented by Greek National Annexes [16]. Accordingly, 33 combinations of actions required in total, as presented in Table 1, where G stands for dead loads, Q for imposed loads and E for seismic loads to primary directions with accidental eccentricities to perpendicular directions.

$A = 1.35G + 1.50Q,$	$I = 1, 2, 3, 4$
${}_iB = 1.00G + 0.30Q + 1.00E_{x\pm eccy} + 0.30E_{y\pm eccx},$	${}_iC = 1.00G + 0.30Q + 1.00E_{x\pm eccy} - 0.30E_{y\pm eccx},$
${}_iD = 1.00G + 0.30Q + 0.30E_{x\pm eccy} + 1.00E_{y\pm eccx},$	${}_iE = 1.00G + 0.30Q - 0.30\,E_{x\pm eccy} + 1.00E_{y\pm eccx},$
${}_iF = 1.00G + 0.30Q - 1.00E_{x\pm eccy} - 0.30E_{y\pm eccx},$	${}_iG = 1.00G + 0.30Q - 1.00E_{x\pm eccy} + 0.30E_{y\pm eccx},$
${}_iH = 1.00G + 0.30Q - 0.30E_{x\pm eccy} - 1.00E_{y\pm eccx},$	${}_iI = 1.00G + 0.30Q + 0.30\,E_{x\pm eccy} - 1.00\,E_{y\pm eccx},$

Table 1: The 33 combinations of actions required.

Comb.	$\mathbf{e_x}$ (m)	$\mathbf{e_y}$ (m)	$\mathbf{p_m}$ (kPa)	$\mathbf{p_1}$ (kPa)	$\mathbf{p_2}$ (kPa)	$\mathbf{p_3}$ (kPa)	$\mathbf{p_4}$ (kPa)	$\mathbf{V_{xf}}$ (kN)	$\mathbf{V_{yf}}$ (kN)	$\mathbf{M_{xf}}$ (kNm)	$\mathbf{M_{yf}}$ (kNm)
A	0.000	0.000	23.2	23.2	23.2	23.2	23.2	8.7	8.7	1.6	1.6
${}_{1,2,3,4}B$	-0.076	-0.003	17.2	7.2	22.5	27.1	11.8	9.1	9.7	1.8	1.8
${}_{1,2,3,4}C$	-0.076	0.003	17.2	11.8	27.1	22.5	7.2	9.1	9.7	1.8	1.8
${}_{1,2,3,4}D$	-0.003	-0.076	17.2	7.2	11.8	27.1	22.5	9.7	9.1	1.8	1.8
${}_{1,2,3,4}E$	0.003	-0.076	17.2	11.8	7.2	22.5	27.1	9.7	9.1	1.8	1.8
${}_{1,2,3,4}F$	0.076	0.003	17.2	27.1	11.8	7.2	22.5	9.1	9.7	1.8	1.8
${}_{1,2,3,4}G$	0.076	-0.003	17.2	22.5	7.2	11.8	27.1	9.1	9.7	1.8	1.8
${}_{1,2,3,4}H$	0.003	0.076	17.2	27.1	22.5	7.2	11.8	9.7	9.1	1.8	1.8
${}_{1,2,3,4}I$	-0.003	0.076	17.2	22.5	27.1	11.8	7.2	9.7	9.1	1.8	1.8

Table 2: Effective eccentricities and resultants for the square central footing for all combinations.

Since no imposed loads exist (Q=0) and no accidental eccentricities considered in this example (ecc_x=ecc_y=0), only 9 out of the 33 combinations are different. The effective eccentricities e_x, e_y, the mean soil pressure p_m, the soil pressure at the corners p_1, p_2, p_3, p_4 and the maximum shearing forces V_{xf}, V_{yf} and bending moments M_{xf}, M_{yf}, are presented in Table 2. It must be underlined that the effective eccentricities have been calculated using equations (2),

the soil pressure values via the explicit formulas applicable in different eccentricity regions along with mapping equations (12), while the rest of the resultants through algebraic integration of soil pressure distribution provided by equation (14). Notice that all combinations, but 'A', impose effective eccentricities despite the fact the footing itself has no structural eccentricity. This was expected since 'A' is the only combination formed exclusively by vertical loads while only horizontal loads can generate rotational reactions in central footings. The soil pressure distributions for different combinations and their envelope are illustrated in Figure 12, while the resultants presented in Table 2 and their envelopes are also shown in Figure 13.

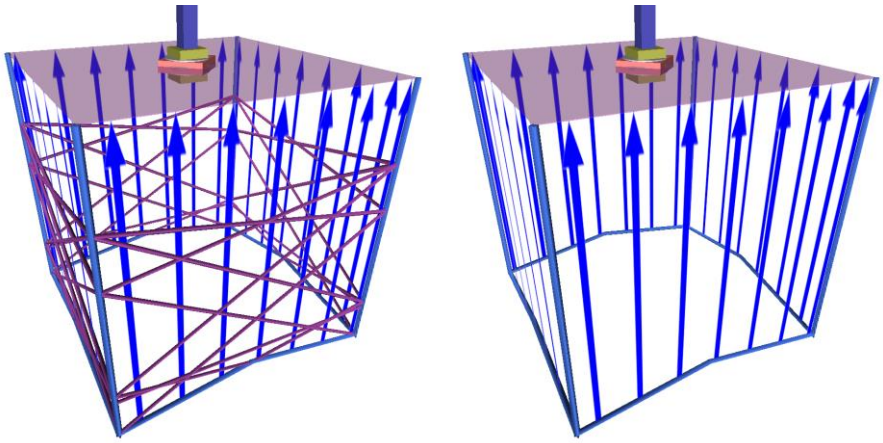

Figure 12: Soil pressure distributions for different combinations and envelope.

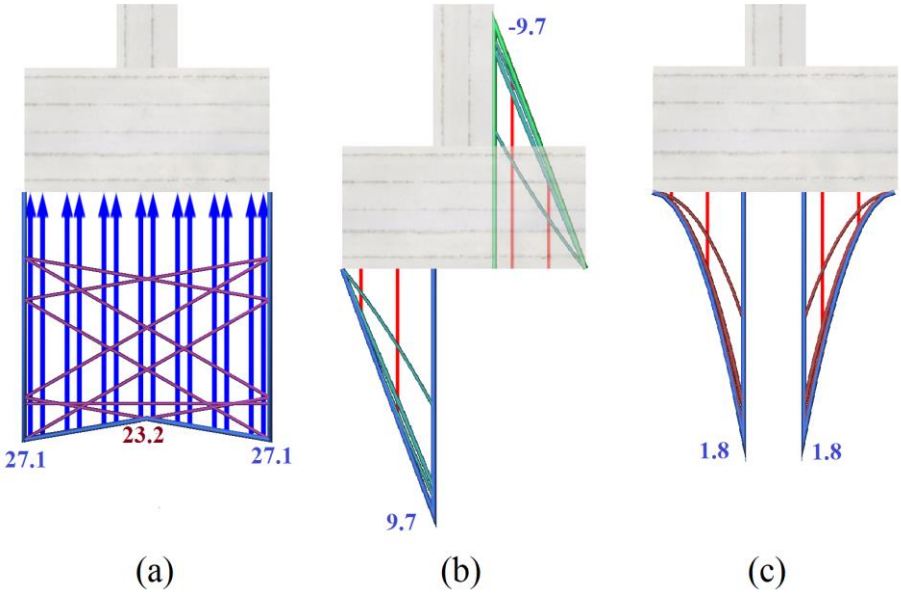

Figure 13: Resultants for different combinations and envelopes:
(a) Soil pressure, (b) Shear forces, (c) Bending moments.

The footing is also studied for variable structural eccentricity with respect to the column. The enveloped maxima of bending moments, namely M_{xd}, M_{yd}, are presented in Figure 14 as a function of structural eccentricity in x-direction. They are also called design bending moments since they are associated with footing design. Notice that only for central footings the two bending components are identical. In fact, by increasing structural eccentricity bending is affected substantially in the direction of structural eccentricity and slightly in the perpendicular direction. This reflects directly on the calculated two-way reinforcement A_{sx}, A_{sy}, shown in

Figure 15 as a function of structural eccentricity in x-direction, where required reinforcement increases substantially in the direction of structural eccentricity.

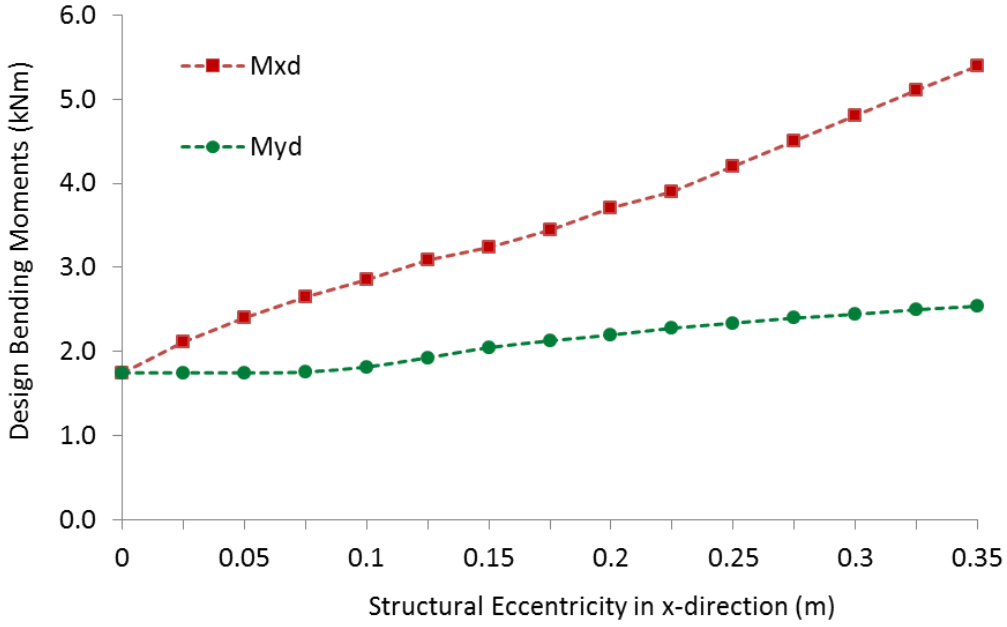

Figure 14: Design bending moments in relation to structural eccentricity in x-direction.

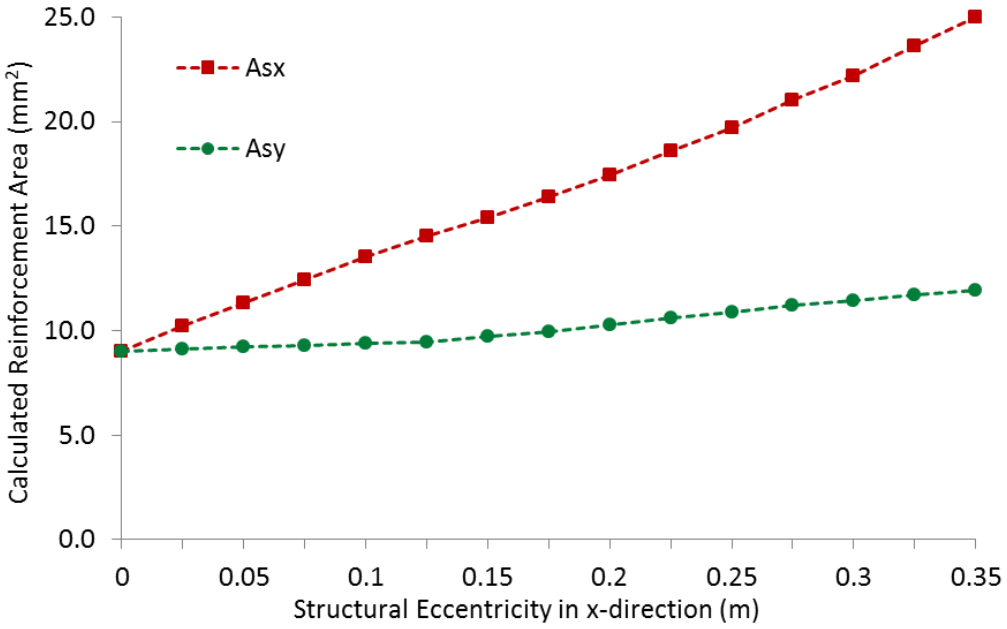

Figure 15: Calculated two-way reinforcement in relation to structural eccentricity in x-direction.

By analyzing the above outcomes, it is clear that there is a substantial amount of calculations involved in the design of rigid spread footings geometry and reinforcement, even if a limited number of combinations is taken into account. Of course, the numbers increase dramatically when optimization is attempted via iterative procedures or when one seeks resultants for multi footings foundations (see Figure 16). In such cases, the explicit formulas revealed in this article are certainly preferable over numerical methods or similar techniques, since they undoubtedly limit computational costs. Furthermore, the proposed here analytical

method is applicable to either a single footing case or a multi footings and connecting beams assembly. Only resultant reactions retrieved from the space frame model are used as input in equations (2), and therefore the process is independent from linked neighboring components.

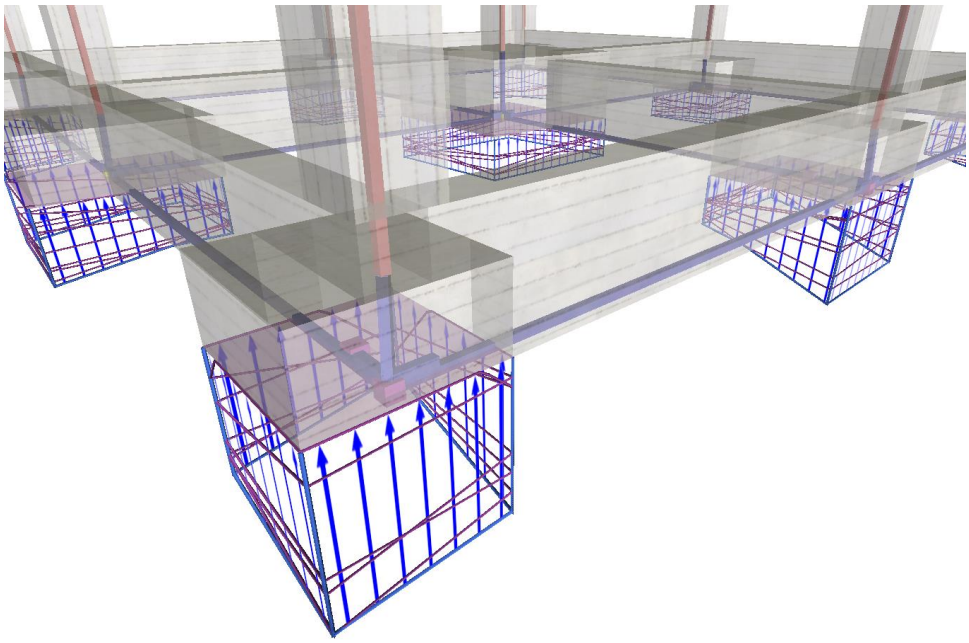

Figure 16: Soil pressure distributions and envelopes for a multi rigid spread rectangular footings foundation.

7 CONCLUSIONS

This article adds value in studying rigid spread rectangular footings resting on elastic soils by offering:

1. High computational efficiency through developed explicit formulas for soil pressure values in different eccentricity regions.
2. A generic, robust and effective solution, independent of the foundation layout, by using as input the reactions computed at the supports instead of actual loads on the footing.
3. An eccentricity diagram per footing, as a very practical qualitative tool for predetermining the form of soil pressure distribution and footing deformation expected.
4. An integrated virtual reality software, facilitating visual examination and validation of the results.

The innovative and straightforward research approach followed here will assist future researchers by providing a valuable reference through a powerful research software tool. Potentially, it could be extended to accounting for more generic footing geometries and non-linear soil pressure distributions.

ACKNOWLEDGEMENTS

The authors would like to express their gratitude to pi-Systems International S.A. for the constant financial support provided during the project, the Institute of Structural Analysis and Seismic Research of National Technical University of Athens for the contribution in developing the computational algorithms for the space frame model and all associates involved in the production of the integrated virtual reality software.

NOTATION

A	Active area of footing
P	Vertical force reaction on footing
M_x, M_y	Rotational moment reactions on footing in x and y directions
$p(x, y)$	Soil pressure distribution
p_1, p_2, p_3, p_4	Soil pressure values on footing corners
p_o, p_p, p_q, p_r	Soil pressure values on rearranged footing corners
p_{max}	Maximum soil pressure value on footing
p_{min}	Minimum soil pressure value on footing
p_m	Mean soil pressure value on footing
l_x, l_y	Footing dimensions in x and y directions
e_x, e_y	Effective eccentricities from footing center in x and y directions
x_c, y_c	Coordinates of footing base centroid
x_n, y_n	Neutral axis intercepts on x and y axes
x, y, z	Coordinate system with origin on footing corner
x', y', z'	Coordinate system with origin on footing centroid
$sign( )$	Sign of a real number
V_{xf}, V_{yf}	Maximum values of shear forces on footing in x and y directions
M_{xf}, M_{yf}	Maximum values of bending moments on footing in x and y directions
M_{xd}, M_{yd}	Design bending moments of footing in x and y directions
A_{sx}, A_{sy}	Calculated steel reinforcement of footing in x and y directions

REFERENCES

[1] J. E. Bowles, *Foundation Analysis and Design, 3rd Edition*. McGraw Hill, New York, 1977.

[2] R. Jarquio, V. Jarquio, Design of Footing Area with Biaxial Bending. *Journal of Geotechnical Engineering,* 109, 1337-1341, 1983.

[3] W. H. Highther, J. C. Anders, Dimensioning Footings Subjected to Eccentric Loads. *Journal of Geotechnical Engineering*, 111, 659-665, 1985.

[4] D. M. Vitone, A. J. Valsangkar, Stresses from Loads over Rectangular Areas. *Journal of Geotechnical Engineering Division*, 112, 961-964, 1986.

[5] R. Irles, F. Irles, Explicit Stresses under Rectangular Footings. *Journal of Geotechnical Engineering*, 120, 444–450, 1994.

[6] H. M. Algin, Stresses from Linearly Distributed Pressures over Rectangular Areas. *International Journal of Numerical Analysis Methods in Geomechanics*, 24, 681–692, 2000.

[7] H. M. Algin, Practical Formula for Dimensioning a Rectangular Footing. *Engineering Structures*, 29, 1128-1134, 2007.

[8] J. P. Smith-Pardo, A. Bobet, Behavior of Rigid Footings on Gravel under Axial Load and Moment. *Journal of Geotechnical and Geoenvironmental Engineering*, 133, 1203–1215, 2007.

[9] N., Yamamoto, M. F. Randolph, I. Einav, Simple Formulas for the Response of Shallow Foundations on Compressible Sands. *International Journal of Geomechanics*, 8, 230–239, 2008.

[10] M. H. T. Rayhani, M. H. El Naggar, Numerical Modeling of Seismic Response of Rigid Foundation on Soft Soil. *International Journal of Geomechanics*, 8, 336–346, 2008.

[11] A. Ivan, Pressures Distribution for Eccentrically Loaded Rectangular Footings on Elastic Soils. *Proceedings of the 2010 International Conference on Mathematical Models for Engineering Science*, 213-216, 2010.

[12] N. S. V. Kameswara Rao, *Analysis of Footings on Elastic Foundations, Chapter 5, Foundation Design: Theory and Practice*. John Wiley & Sons (Asia) Pte Ltd, 165–202, 2011.

[13] G. Özmen, Determination of Base Stresses in Rectangular Footings under Biaxial Bending. *Teknik Dergi*, 22, 5659-5674, 2011.

[14] A. L. Rojas, J. G. F. Herrera, R. A. A. Vallejo and M. A. C. Alvarez, Design of Isolated Footings of Rectangular Form Using a New Model. *International Journal of Innovative Computing, Information and Control*, 9, 4001-4021, 2013.

[15] J. A. Rodriguez-Gutierrez, J. D. Aristizabal-Ochoa, Rigid Spread Footings Resting on Soil Subjected to Axial Load and Biaxial Bending. II: Design Aids. *International Journal of Geomechanics*, 13, 109-119, 2013.

[16] A. Konstantinides, J. Bellos, *Earthquake Resistant Buildings made of Reinforced Concrete: Static and Dynamic Analysis according to Eurocodes, Volume B*. Alta Grafico, Athens, 2013.